Published in final edited form as:
Radiother Oncol. 2008 April ; 87(1): 35–43. doi:10.1016/j.radonc.2008.02.010.

An evaluation of planning techniques for stereotactic body radiation therapy in lung tumors

Jianzhou Wu, PhD[1,2], **Huiling Li, MD**[1], **Raj Shekhar, PhD**[2], **Mohan Suntharalingam, MD**[1], and **Warren D'Souza, PhD**[1]

[1]Department of Radiation Oncology, University of Maryland School of Medicine, Baltimore, MD 21201

[2]Department of Diagnostic Radiology, University of Maryland School of Medicine, Baltimore, MD 21201

Abstract

Purpose—To evaluate four planning techniques for stereotactic body radiation therapy (SBRT) in lung tumors.

Methods and Materials—Four SBRT plans were performed for 12 patients with stage I/II non-small-cell lung cancer under the following conditions: (1) conventional margins on free-breathing CT (plan 1), (2) generation of an internal target volume (ITV) using 4DCT with beam delivery under free-breathing conditions (plan 2), (3) gating at end-exhale (plan 3), and (4) gating at end-inhale (plan 4). Planning was performed following the RTOG 0236 protocol with a prescription dose of 54Gy (3 fractions). For each plan 4D dose was calculated using deformable image registration.

Results—There was no significant difference in tumor dose delivered by the 4 plans. However, compared with plan 1, plans 2-4 reduced total lung BED by 1.9±1.2Gy, 3.1±1.6Gy and 3.5±2.1Gy, reduced mean lung dose by 0.8±0.5Gy, 1.5±0.8Gy, and 1.6±1.0Gy, reduced V20 by 1.5±1.0%, 2.7 ±1.4%, and 2.8±1.8% respectively with $p<0.01$. Compared with plan 2, plans 3-4 reduced lung BED by 1.2±1.0Gy and 1.6±1.5Gy, reduced mean lung dose by 0.6±0.5Gy and 0.8±0.7Gy, reduced V20 by 1.2±1.1% and 1.3±1.5% respectively with $p<0.01$. The differences in lung BED, mean dose and V20 of plan 4 compared with plan 3 are insignificant.

Conclusions—Tumor dose coverage was statistically insignificant between all plans. However, compared with plan 1, plans 2-4 significantly reduced lung doses. Compared with plan 2, plan 3-4 also reduced lung toxicity. The difference in lung doses between plan 3 and plan 4 was not significant.

Keywords

image registration; 4D dose; SBRT; lung tumor

Introduction

Stereotactic body radiation therapy (SBRT) is emerging as an efficient treatment for Stage I/II medical inoperable and surgically unresectable non-small-cell and metastatic lung cancer

Correspondence: Warren D. D'Souza, PhD, Department of Radiation Oncology, University of Maryland Medical Center, 22 South Greene St, Baltimore, MD 21201, Tel: 410-328-7159, Fax: 410-328-2618.

Partially presented at the 49th AAPM Annual Meeting, Minneapolis, MN

Conflict of Interest Statement: Conflicts of interest do not exist.

[1-12]. Dose escalation and hypofractional dose delivery has the potential to increase patients' survival rates [3] and the probability of local tumor control [4,6,8], while increasing median survival time and long-term progression-free survival [7]. The first dose-response in pulmonary SBRT was reported by Wulf *et al* [5]. However, respiration-induced motion can be significant in lung tumors and can result in discrepancies between the planned and delivered doses [13-15]. To more accurately calculate the dose delivered in the case of lung tumors, anatomical motion must be accounted for during treatment planning.

Conventional treatment plans for SBRT of lung tumors are performed on free breathing 3D CT images. Free-breathing CT images are susceptible to motion artifacts, hence, the GTVs delineated on the free-breathing images may inaccurately estimate the position and volume of the tumor and critical structures. Treatment plans using the GTVs delineated on the free-breathing images ignore tumor motion information. Hence, safety margins are added to create the planning target volume (PTV) in order to avoid geometrical misses of the target. Consequently the volume of healthy tissues irradiated increases.

In contrast, 4D CT imaging enables the delineation of temporal anatomic translation and deformation information on 3D CT image sets corresponding to various phases of the respiration cycle. Consequently the GTVs delineated on the 4D CT images represent more accurately the tumor shape, volume and position [16-17]. The individual target volumes can be combined to form and internal target volume (ITV) [18]. The corresponding PTV was formed by adding a margin that would account for daily setup uncertainties. While both of the above target definition methods assume that the treatment is delivered under free-breathing conditions, more sophisticated delivery methods such as gating are becoming commonplace in clinical treatments. However, reports describing a planning infrastructure for gated treatments based on 4D CT images are limited [19].

Irrespective of planning and delivery methods, the dose distribution typically evaluated clinically is a 3D dose calculated on a single CT image. In reality, organs move due to respiration and the corresponding 4D dose is largely ignored. Several methods have been proposed for 4D dose calculation [15,20-23]. Lujan *et al.* [20] and Bortfeld *et al.* [21] described an approach involving the convolution of the static dose distribution with the probability distribution function (PDF) of the organ's motion. Craig *et al* [22] however, showed that the assumption of "shift invariance" in such calculations can produce artifacts in regions with sharp discontinuities such as the patient's surface or in regions with inhomogeneities. Fluence-based methods, in which the fluence is convolved with the PDF of the organ's motion, are not susceptible to such artifacts. Beckham *et al* [23] and Chetty *et al* [24] calculated 4D dose by convolving the fluence with the PDF. Naqvi and D'Souza developed a stochastic method for calculating the expectation 4D dose distribution from a large number of treatment fractions in which the isocenter traces the trajectory of the organ [15]. However, none of the above approaches considered anatomical deformation.

Recently, more advanced techniques have been used for 4D dose calculation [12,19,25-26], and are based on the elastic registration of the 4D CT images. Elastic image registration tracks the displacement of each voxel during a respiratory cycle. The dose summed along the trajectory of each voxel provides a more accurate estimate of 4D dose. This method explicitly takes into account the relative anatomic changes in shape, volume, position, and density during normal respiration. Rietzel *et al.* calculated dose for patients with thoracic and hepatocellular tumors by performing B-splines based deformable image registration using an open source software package [25]. Guerrero *et al.* developed a 3D optical flow-based elastic registration algorithm and calculated the 4D dose distribution using a computer-generated 4D thoracic phantom [26]. However, this study was limited to phantom images. Flampouri *et al.* estimated the dose delivered from IMRT to lung tumor patients based on elastic image registration of 4D

CT [19]. However, these studies considered only conventional fractionation schemes. Guckenberger *et al*. investigated the influence of tumor motion on the dose delivery of lung SBRT [12]. However, they studied only one delivery scenario: free breathing with ITV-based treatment planning.

Since hypofractionation and more sophisticated delivery methods (such as gating) are being increasingly considered for early-stage lung tumors, it becomes necessary to calculate more accurately estimates of the dose in the presence of respiration-induced tumor motion. The Radiation Therapy Oncology Group (RTOG) recently concluded a national trial for hypofractionated delivery in medically inoperable and surgically unresectable lung tumors (protocol # RTOG 0236). At our institution, a similar trial has been underway. In this work, we retrospectively compared the 4D dose calculated under four different treatment planning and delivery scenarios for SBRT treatments of lung tumors. The four treatment planning and delivery techniques were evaluated by comparing their corresponding composite 4D dose distributions.

Methods and materials

Twelve lung cancer patients who underwent hypofractionated radiotherapy at our institution were retrospectively selected for this study. Each patient underwent a 4D simulation using the Brilliance multi-slice CT scanner (Philips Medical Systems, Cleveland, OH) with the respiration phase inferred using an infrared marker/camera system (RPM system, Varian Medical Systems, Palo Alto, CA). Each 4D CT data set comprised ten 3D CT images corresponding to equally spaced phases in the respiratory cycle.

For each patient, we performed treatment planning according to the guidelines in the RTOG 0236 protocol [27]. The prescription dose however at our institution (using our institutional protocol) was set to 18 Gy/fraction for a total of 3 fractions. We will briefly summarize the planning parameters and constraints here. All plans were normalized such that 54 Gy was prescribed to the 85% isodose line. The maximum point dose to the heart, trachea and ipsilateral bronchus was required to be less than 30 Gy; the maximum point doses to the spinal cord, esophagus, and ipsilateral brachial plexus were required to be less than 18 Gy, 27 Gy and 24 Gy, respectively; V20 of the total lung (ipsilateral and contralateral lung) volume was required to be less than 15%. All of these requirements and constraints were satisfied for all of the plans.

The monitor units (MU) were determined by assuming homogeneous patient geometry (as required by RTOG 0236). However, the final dose calculations including the effective 4D dose calculations described below were performed using heterogeneity corrections. This was done by first recording the MUs of each beam from the original plans performed with homogeneous assumption. The plan parameters were then copied to each individual 4D CT images to recalculate the dose with heterogeneity correction using the MUs obtained from the homogeneous plan. A convolution/superposition algorithm implemented by the Pinnacle^3 planning system (Philips Medical Systems, Cleveland, OH) was used for dose calculation. Convolution/superposition algorithm has been shown be in agreement with Monte Carlo (MC) simulation for dose calculation in heterogeneous media [28-30].

Four treatment plans were generated for each patient case. Each treatment plan simulated a different planning and delivery scenario. Table 1 summarizes these four SBRT plans. In plan 1, a 5 mm margin in the anterior-posterior (AP) and medial-lateral (ML) directions and a 10 mm margin in the cranio-caudal (CC) direction was added to the GTV contoured on the free-breathing (FB) CT image set to create the PTV. In plan 2, the GTV was delineated on each of the 3D CT data sets in the 4D CT. These GTV volumes were combined to yield an ITV. A uniform 5 mm margin was then added to the ITV to form the PTV, which was then imported

onto the FB CT. In both, plans 1 and 2, planning was performed on the FB CT. However, unlike plan 1, plan 2 takes into account respiration induced tumor motion. These two plans correspond to radiation delivery under free-breathing conditions. Plans 3 and 4 were generated to simulate gating at end-exhale and end-inhale, respectively. Phase-based gating was assumed with a 30% duty cycle. In plan 3, the GTVs in the 4D CT data set that fell within the 30% duty cycle centered at end-exhale were combined to form an ITV_{ex}. In our work end-exhale was determined by locating the 3D CT in the 4D CT data set corresponding to the superior-most location of the center-of-mass of the tumor volume. The center of the phase bin in the RPM marker data corresponding to the "end-exhale" CT was assigned the status of "end-exhale". The phase-based gating window was then determined relative to this center. A 5 mm margin was added to ITV_{ex} to generate a PTV_{ex}. Planning in plan 3 was performed on the CT data set corresponding to end-exhale in the respiration cycle. In plan 4, the same process was repeated with the gating window centered at end-inhale to generate ITV_{in}. A 5 mm margin was added to generate a PTV_{in} with the gating window determined in a similar manner as described above. Planning in plan 4 was performed on the CT data set corresponding to end-inhale in the respiration cycle.

The calculation of 4D dose under each planning and delivery scenario consisted of a three-step process. The first step was to recalculate the dose distribution on each individual 3D CT image with tissue heterogeneity correction. This step was performed by superimposing the plan parameters obtained from assuming homogeneous geometry onto each of the individual 3D CT images in the 4D data set (for plans 3 and 4, the parameters were copied onto the CT images that were within the phase-based gating window). During the copying of the plan parameters, the isocenter position was invariant in the room coordinate system between the individual 3D CT image data sets. For plans 1 and 2, all of the 10 individual 3D CT images were used to recalculate the dose. For plans 3 and 4, there were typically 3-5 CT data sets (depending on the patient case) located within the 30% gating window.

The second step in the 4D dose calculation process involved image registration. The objective here was to find the displacement trajectory of each voxel. The displacement of each voxel with respect to a reference image set (the reference image set in this study corresponded to end-exhale) was obtained by registering each of the 3D CT images in the 4D CT to the reference CT image set. The image registration algorithm used in this study was a previously published elastic registration algorithm [31]. Details of the algorithm can be found in the above reference but are briefly summarized here. This algorithm models tissue deformation by a B-spline based free-form deformation (FFD), defined by a linear combination of a cubic B-spline placed on a regular 3D grid of control points in the reference image space. An advantage of using a B-spline is that moving a control point affects only a subset of voxels in its neighborhood. The objective function in the image registration algorithm was the mean-squared difference (MSD) in intensity, which was minimized during the optimization procedure. A novel 3D ChainMail algorithm was introduced to preserve the grid topology and allow fast registration. The output transformation field specified the displacement of control points. The voxel displacement was obtained by the B-splines based cubic interpolation of the coordinates of the control points in the voxel's neighborhood. The accuracy of this algorithm in the thoracic anatomy has been previously reported [31].

The last step in the process of calculating the 4D dose was dose registration. The dose calculated on 3D CT data sets in the 4D CT image sets was weighted according to the temporal probability derived from the respiration signal corresponding to the time the x-rays were on during CT projection acquisition. Dose registration was performed by first warping each recalculated and weighted dose distribution in step 1 to the reference CT and then using the transformation fields saved from the image registration process. In plans 1, 2 and 3, the reference CT was the 3D CT corresponding to end-exhale in the respiration cycle, while in plan 4, the reference CT was

that corresponding to end-inhale in the respiration cycle. The registered dose distributions were then summed to yield the 4D dose distribution corresponding to each of the 4 planning and delivery scenarios. The entire process of 4D dose calculation is summarized in Fig. 1.

The 4D doses resulting from the 4 plans were analyzed and compared in terms of physical and biological measures, i.e., dose-volume measures, homogeneity index (HI) of the tumor dose, mean biologically effective dose (BED), mean normalized total dose (NTD), lung V20 (volume of the lung receiving 20 Gy) and mean lung dose (MLD). The HI describes the uniformity of the dose within a target volume and is defined as $HI = D_{5\%} / D_{95\%}$, where $D_{5\%}$ and $D_{95\%}$ denote the dose received by 5% and 95%, respectively, of the target volume. The local BED is defined as the total dose×$(1 + d /(\alpha/\beta))$, where d is the local dose (in one voxel) per fraction, α/β was taken as 10 Gy for tumor and 3 Gy for normal lung tissue [32] The mean BED was obtained by averaging local BEDs over the whole corresponding structures. NTD in this study was defined as the normalized total dose delivered in 2 Gy per fraction, $NTD = BED/(1 +2Gy/(\alpha/\beta))$. The MLD has been shown to be a good predictor of the radiation-induced lung pneumonitis [33].

Results

Table 2 lists the tumor volume at end-exhale, tumor location, and peak-to-peak motion of the 12 patients. The minimum peak-to-peak motion for the patients considered in this work was 0.8 cm. Table 1 also lists the volumes of the GTV_{FB} (plan 1), ITV (plans 2-4), and PTV for the 4 plans averaged over all 12 patients. On average the volumes of the ITV used in plans 2-4 were 1.11 ± 0.08 , 0.76 ± 0.07 and 0.79 ± 0.09 times of the volume GTV_{FB} used in plan 1, respectively. The corresponding ratios of the PTV volumes in plans 2-4 with respect to the PTV in plan 1 were 0.89 ± 0.06 , 0.68 ± 0.06 and 0.70 ± 0.06 , respectively.

Figure 2 shows the isodose lines (100%, 85%, 50%, and 20%) for a representative patient of (a) plan 1 on FB CT, (b) plan 2 on FB CT, (c) plan 3 on the end-exhale CT, (d) plan 4 on the end-inhale CT. The thick black curves are the GTVs at end-exhale for plan 1-3 and GTV at end-inhale for plan 4. The thick gray curves are GTV_{FB}, ITV, ITV_{ex}, and ITV_{in} respectively. Even though respiration induced tumor motion smears the dose distribution, the GTV coverage is adequate for all of the 4 plans. Figure 2 (e) demonstrates the DVHs of the composite 4D dose evaluated on the end-exhale CT (plan 1-3) and end-inhale CT (plan 4) for the representative patient. The dose received by 100% of the GTV was at least 54.4 Gy, 58.2 Gy, 59.8 Gy, and 58.7 Gy, respectively for plans 1-4, hence all of the 4 plans can deliver the prescribed dose to the tumor. The HIs of the 4 plans were 1.044, 1.055, 1.079 and 1.058, respectively. The maximum difference in HI between plan 1 and plans 2-4 was less than 3.4%. However, the V10 and V20, percent lung volume receiving 10 Gy and 20 Gy respectively, had large differences among the 4 plans. Plan 1 delivered the highest V10 (29.0%) and V20 (14.1%). In comparison, plan 3 delivered the lowest V10 (20.4%) and V20 (10.4%). In this study, dose was renormalized to 85% isodose line for all the plans and all the patients (as per the recommendations of the RTOG 0236 protocol). Normally 97% or higher of the PTV was covered by the prescribed dose. The volume of the PTV determines the mean dose received by the lung. Since plan 1 used the largest PTV, as a result, it delivered the highest dose (V10 and V20) to the lung with respect to the rest 3 plans.

Figure 3 demonstrates the mean tumor BED and NTD resulting from 4 plans for the 12 patients. The difference in tumor BED among the 4 plans was small, as shown in Table 3, which lists the absolute change in the mean tumor BED and NTD for plans 2-4 relative to plan 1. On average plan 2 reduced the mean tumor BED by 4.0±6.2 Gy ($p = 0.05$), while gating at end-exhale increased it by 0.9±7.6 Gy ($p = 0.69$), and gating at end-inhale increased it by 1.0±7.2

Gy (p = 0.63). The absolute change in tumor BED of plans 2-4 with respect to plan 1 was statistically insignificant. Similar statistics were observed for NTD of the 4 plans.

Figure 4 shows the mean BED, mean lung dose, and V20 of the total lung (contralateral + ipsilateral lung) and the ipsilateral lung of the 4 plans for the 12 patients. The averaged reductions in mean lung BED, NTD, mean dose, and V20 of plans 2-4 with respect to the plan 1 are listed in Table 3. On average, with respect to plan 1, plans 2-4 reduced the total lung BED by 1.9±1.2 Gy ($p < 0.01$), 3.1±1.6 Gy ($p < 0.01$), and 3.5±2.1 Gy ($p < 0.01$), respectively, reduced the mean total lung dose by 0.8±0.5 Gy ($p < 0.01$), 1.5±0.8 Gy ($p < 0.01$), and 1.6±1.0 Gy ($p < 0.01$) respectively, and reduced the total lung V20 by 1.5±1.0% ($p < 0.01$), 2.7±1.4% ($p = 0.01$), and 2.8±1.8% ($p < 0.01$) respectively. For the ipsilateral lung, the corresponding reductions in BED were 3.4±2.0 Gy ($p < 0.01$), 5.4±2.9 Gy ($p < 0.01$), and 6.2±3.9 Gy ($p < 0.01$), respectively, the reduction in the mean lung dose were -0.9±1.3 (p=0.04), -2.1±1.3 (p<0.01), and -2.5±1.9 (p<0.01) respectively, and the reduction in ipsilateral lung V20 were -2.7±1.7 (p<0.01), -4.9±2.6 (p<0.01), and -5.2±3.7 (p<0.01) respectively.

Table 4 lists the absolute difference in mean BED, mean NTD, mean delivered dose of the tumors, mean BED, mean NTD, mean delivered dose, and V20 of the total lungs and ispilateral lungs of plans 3-4 with respect to plan 2, and for plan 4 with respect to plan 3, averaged over the 12 patients. Compared with the ITV-based free-breathing planning technique (plan 2), gating (plan 3-4) improved tumor BED by 4.9±10.6 Gy (p=0.14) and 5.0±5.8 Gy (p=0.01) respectively. The reductions in total lung BED were 1.2±1.0Gy (p<0.01) and 1.6±1.5Gy (p<0.01), the reduction in mean total lung dose were 0.6±0.5Gy (p<0.01) and 0.8±0.7Gy (p<0.01), the reduction in total lung V20 were 1.2±1.1% (p<0.01) respectively. For the ipsilateral lung, the corresponding reduction in BED were 2.1±1.8 Gy (p<0.01) and 2.9±2.8 Gy (p<0.01), the reduction in mean dose were 1.3±0.9 Gy (p<0.01) and 1.6±1.3 Gy (p<0.01), the reduction in V20 were 2.2±1.8% (p<0.01) and 2.5±2.9% (p=0.01) respectively. The differences in tumor BED, lung BED, mean lung dose and lung V20 were not significant ($p=0.19$), which indicated that there was no statistical difference between gating at end-inhale and gating at end-exhale.

DISCUSSION

The purpose of this paper was to retrospectively evaluate four different treatment planning scenarios for SBRT of lung cancer by following some of the guidelines in the RTOG protocol 0236. While the monitor units were calculated with a homogeneous geometry assumption, the final dose was calculated using heterogeneity correction. Our results show that the difference of tumor dose at different respiration phases is insignificant, which agrees with the conclusion drawn by Guckenberger *et al* [12]. Our results also suggest that there are no statistical differences between tumor coverage between any of the methods investigated. However, there are differences in the lung doses achieved with each of the methods.

Accounting for respiration-induced tumor motion can be approached from two viewpoints: (1) achieving adequate tumor coverage and (2) achieving better normal tissue sparing. For all of the four planning techniques investigated, the difference in tumor BED and NTD was insignificant, which means that all of the four plans performed equally well from the point of view of tumor coverage. However, we did observe significant differences in lung BED, NTD and V20 between plan 1 and the remaining plans. These results reinforce the notion that the rationale for investing in sophisticated motion correction strategies is to achieve better normal tissue sparing.

In our work we considered tumors that exhibited peak-peak motion up to 1.7 cm. For the plans performed on the free-breathing CT without the knowledge of tumor motion, the margins used

to create the PTV are large enough to deliver the prescribed dose to the tumor, even though the peak-to-peak tumor motion is 1.7 cm. Our observation does not agree with that reported by Flampouri *et al* [19]. That paper concluded that treatment planning was not adequate for patients with tumor motion larger than 1.2 cm. The difference in observation is due to dose normalization during treatment planning. In Flampouri *et al*, the IMRT treatment plan, performed on the free-breathing CT image, was renormalized so that 95% of the CTV, not the PTV, gets the prescribed dose. In this study, the prescribed dose was renormalized to the 85% isodose line as per the guidelines of RTOG 0236. Hence the dose coverage of the PTV was typically more than 97% in our study.

While gating is generally performed at end-exhale due to the smaller variability in breathing patterns at end-exhale compared with end-inhale [34-35], there is no dosimetric rationale for selecting the location of the gating window. Our results show that with respect to gating at end-exhale, gating at end-inhale may result in slightly reduced lung dose, however, the reductions in lung BED and NTD are on average ≤0.4 Gy, and these reductions are statistically not significant. Our conclusions are consistent with the results obtained by Biancia *et al* [36]. In Biancia *et al*., IMRT plans performed at end-inhale were compared with plans performed at end-exhale for 10 patients. They found that for plans performed at end-exhale the average mean lung dose and V20 were 16.3 Gy and 25.3% respectively. These dosimetric indices were reduced to 15.4 Gy and 23.8 % respectively for plans performed at end-inhale. They concluded that the improvement in lung protection was small.

Since the treatment plans in this study were performed on the CT scans obtained on a single simulation day, the above discussion intrinsically assumed the inter-fraction respiration patterns were reproducible. However, previous investigators have shown slight variability in respiration between fractions [37-41]. We believe that the logical next step is to take into consideration 4D CT scans acquired on multiple days. By considering the variation in daily respiration patterns, we speculate that margins might need to be expanded. To minimize the influence of respiration variability, an appropriate margin, accounting for the inter-fraction variation in respiration pattern could be added to ITV, ITV_{ex} or ITV_{in} when creating the corresponding PTVs. However, with the expansion in margins, it remains to be seen whether the differences/similarities between plans 1-4 still hold. Alternatively, to ensure more reproducible respiration patterns between fractions one can use of coaching aids [42]. It has been reported that the efficiency and reproducibility of gating can be improved by using an audio-visual biofeedback system [42].

Conclusions

We have compared the SBRT in lung tumors for 4 different planning scenarios retrospectively. The margins used in the 4 plans were adequate to compensate for respiration induced organ motion in SBRT delivery for lung tumors. Plans created on the free-breathing CT images without the knowledge of tumor motion use the largest margins and consequently, the lung BED, NTD and V20 were the highest among the four plans evaluated in this paper. To reduce the lung dose and toxicity, organ motion information should be considered during treatment planning using either an ITV approach or gated delivery. Gating at end-inhale and end-exhale, respectively produced no statistical differences in tumor and lung dosimetry.

Acknowledgments

This work was supported in part by a grant from NCI/NIH CA 122403.

References

1. Uematsu M, Shioda A, Suda A, et al. Computed tomography-guided frameless stereotactic radiotherapy for stage I non-small cell lung cancer: a 5-year experience. Int J Radiat Oncol Biol Phys 2001;51:666–670. [PubMed: 11597807]
2. Nagata Y, Negoro Y, Aoki T, et al. Clinical outcomes of 3D conformal hypofractionated single high-dose radiotherapy for one or two lung tumors using a stereotactic body frame. Int J Radiat Oncol Biol Phys 2002;52:1041–1046. [PubMed: 11958900]
3. Onishi H, Araki T, Shirato H, et al. Stereotactic hypofractionated high-dose irradiation for stage I nonsmall cell lung carcinoma: clinical outcomes in 245 subjects in a Japanese multiinstitutional study. Cancer 2004;101:1623–1631. [PubMed: 15378503]
4. McGarry RC, Papiez L, Williams M, et al. Stereotactic body radiation therapy of early-stage non-small-cell lung carcinoma: phase I study. Int J Radiat Oncol Biol Phys 2005;63:1010–1015. [PubMed: 16115740]
5. Wulf J, Baier K, Mueller G, et al. Dose-response in stereotactic irradiation of lung tumors. Radiother Oncol 2005;77:83–87. [PubMed: 16209896]
6. Joyner M, Salter BJ, Papanikolaou N, et al. Stereotactic body radiation therapy for centrally located lung lesions. Acta Oncol 2006;45:802–807. [PubMed: 16982543]
7. Okunieff P, Petersen AL, Philip A, et al. Stereotactic Body Radiation Therapy (SBRT) for lung metastases. Acta Oncol 2006;45:808–817. [PubMed: 16982544]
8. Hoyer M, Roed H, Hansen AT, et al. Prospective study on stereotactic radiotherapy of limited-stage non–small-cell lung cancer. Int J Radiat Oncol Biol Phys 2006;66:S128–S135.
9. Jin JY, Ajlouni M, Chen Q, et al. Quantification of incidental dose to potential clinical target volume (CTV) under different stereotactic body radiation therapy (SBRT) techniques for non-small cell lung cancer - Tumor motion and using internal target volume (ITV) could improve dose distribution in CTV. Radiother Oncol 2007;85:267–276. [PubMed: 17905457]
10. Koto M, Takai Y, Ogawa Y, et al. A phase II study on stereotactic body radiotherapy for stage I non-small cell lung cancer. Radiother Oncol 2007;85:429–434. [PubMed: 18022720]
11. Guckenberger M, Heilman K, Wulf J, et al. Pulmonary injury and tumor response after stereotactic body radiotherapy (SBRT): Results of a serial follow-up CT study. Radiother Oncol 2007;85:435–442. [PubMed: 18053602]
12. Guckenberger M, Wilbert J, Krieger T, et al. Four-dimensional treatment planning for stereotactic body radiotherapy. Int J Radiat Oncol Biol Phys 2007;69:276–285. [PubMed: 17707282]
13. George R, Keall PJ, Kini VR, et al. Quantifying the effect of intrafraction motion during breast IMRT planning and dose delivery. Med Phys 2003;30:552–562. [PubMed: 12722807]
14. Chui CS, Yorke E, Hong L. The effects of intra-fraction organ motion on the delivery of intensity-modulated field with a multileaf collimator. Med Phys 2003;30:1736–1746. [PubMed: 12906191]
15. Naqvi SA, D'Souza WD. A stochastic convolution/superposition method with isocenter sampling to evaluate intrafraction motion effects in IMRT. Med Phys 2005;32:1156–1163. [PubMed: 15895599]
16. Pan T, Lee TY, Rietzel E, et al. 4D-CT imaging of a volume influenced by respiratory motion on multi-slice CT. Med Phys 2004;31:333–340. [PubMed: 15000619]
17. Rietzel E, Pan T, Chen GT. Four-dimensional computed tomography: image formation and clinical protocol. Med Phys 2005;32:874–889. [PubMed: 15895570]
18. ICRU Report 62: Prescribing, recording and reporting photon beam therapy (supplement to ICRU report 50). Bethesda: International Commission on Radiation Units and Measurements; 1999.
19. Flampouri S, Jiang SB, Sharp GC, et al. Estimation of the delivered patient dose in lung IMRT treatment based on deformable registration of 4D-CT data and Monte Carlo simulations. Phys Med Biol 2006;51:2763–2779. [PubMed: 16723765]
20. Lujan AE, Larsen EW, Balter JM, et al. A method for incorporating organ motion due to breathing into 3D dose calculations. Med Phys 1999;26:715–720. [PubMed: 10360531]
21. Bortfeld T, Jokivarsi K, Goitein M, et al. Effects of intra-fraction motion on IMRT dose delivery: statistical analysis and simulation. Phys Med Biol 2002;47:2203–2220. [PubMed: 12164582]

22. Craig T, Battista J, Van Dyk J. Limitations of a convolution method for modeling geometric uncertainties in radiation therapy. I. The effect of shift invariance. Med Phys 2003;30:2001–2011. [PubMed: 12945966]
23. Beckham WA, Keall PJ, Siebers JV. A fluence-convolution method to calculate radiation therapy dose distributions that incorporate random set-up error. Phys Med Biol 2002;47:3465–3473. [PubMed: 12408475]
24. Chetty IJ, Rosu M, Tyagi N, et al. A fluence convolution method to account for respiratory motion in three-dimensional dose calculations of the liver: a Monte Carlo study. Med Phys 2003;30:1776–1780. [PubMed: 12906195]
25. Rietzel E, Chen GT, Choi NC, et al. Four-dimensional image-based treatment planning: target volume segmentation and dose calculation in the presence of respiratory motion. Int J Radiat Oncol Biol Phys 2005;61:1535–1550. [PubMed: 15817360]
26. Guerrero T, Zhang G, Segars W, et al. Elastic image mapping for 4-D dose estimation in thoracic radiotherapy. Radiat Prot Dosimetry 2005;115:497–502. [PubMed: 16381774]
27. Radiation Therapy Oncology Group. RTOG 0236 A Phase II Trial of Stereotactic Body Radiation Therapy (SBRT) in the Treatment of Patients with Medically Inoperable Stage I/II Non-Small Cell Lung Cancer. RTOG Headquarters/Statistical Unit; Philadelphia, PA: 2006.
28. Jones AO, Das IJ. Comparison of inhomogeneity correction algorithms in small photon fields. Med Phys 2005;32:766–776. [PubMed: 15839349]
29. Paelinck L, Reynaert N, Thierens H, et al. Experimental verification of lung dose with radiochromic film: comparison with Monte Carlo simulations and commercially available treatment planning systems. Phys Med Biol 2005;50:2055–2069. [PubMed: 15843736]
30. Vanderstraeten B, Reynaert N, Paelinck L, et al. Accuracy of patient dose calculation for lung IMRT: A comparison of Monte Carlo, convolution/superposition, and pencil beam computations. Med Phys 2006;33:3149–3158. [PubMed: 17022207]
31. Shekhar R, Lei P, Castro-Pareja CR, et al. Automatic segmentation of phase-correlated CT scans through nonrigid image registration using geometrically regularized free-form deformation. Med Phys 2007;34:3054–3066. [PubMed: 17822013]
32. Fowler JF, Tomé WA, Fenwick JD, et al. A challenge to traditional radiation oncology. Int J Radiat Oncol Biol Phys 2004;60:1241–56. [PubMed: 15519797]
33. Seppenwoolde Y, Lebesque JV, de Jaeger K, et al. Comparing different NTCP models that predict the incidence of radiation pneumonitis. Normal tissue complication probability. Int J Radiat Oncol Biol Phys 2003;55:724–735. [PubMed: 12573760]
34. Seppenwoolde Y, Shirato H, Kitamura K, et al. Precise and real-time measurement of 3D tumor motion in lung due to breathing and heartbeat, measured during radiotherapy. Int J Radiat Oncol Biol Phys 2002;53:822–834. [PubMed: 12095547]
35. Mageras GS, Yorke E. Deep inspiration breath hold and respiratory gating strategies for reducing organ motion in radiation treatment. Semin Radiat Oncol 2004;14:65–75. [PubMed: 14752734]
36. Biancia CD, Yorke E, Chui CS, et al. Comparison of end normal inspiration and expiration for gated intensity modulated radiation therapy (IMRT) of lung cancer. Radiother Oncol 2005;75:149–156. [PubMed: 16086906]
37. Seppenwoolde Y, Shirato H, Kitamura K, et al. Precise and real-time measurement of 3D tumor motion in lung due to breathing and heartbeat, measured during radiotherapy. Int J Radiat Oncol Biol Phys 2002;53:822–34. [PubMed: 12095547]
38. Erridge SC, Seppenwoolde Y, Muller SH, et al. Portal imaging to assess set-up errors, tumor motion and tumor shrinkage during conformal radiotherapy of non-small cell lung cancer. Radiother Oncol 2003;66:75–85. [PubMed: 12559524]
39. van der Geld YG, Lagerwaard FJ, van Sornsen de Koste JR, et al. Reproducibility of target volumes generated using uncoached 4-dimensional CT scans for peripheral lung cancer. Radiat Oncol 2006;1:43. [PubMed: 17078882]
40. Guckenberger M, Wilbert J, Meyer J, et al. Is a single respiratory correlated 4D-CT study sufficient for evaluation of breathing motion? Int J Radiat Oncol Biol Phys 2007;67:1352–1359. [PubMed: 17394941]

41. Haasbeek CJ, Lagerwaard FJ, Cuijpers JP, et al. Is adaptive treatment planning required for stereotactic radiotherapy of stage I non-small-cell lung cancer? Int J Radiat Oncol Biol Phys 2007;67:1370–1374. [PubMed: 17275206]

42. George R, Chung TD, Vedam SS, et al. Audio-visual biofeedback for respiratory-gated radiotherapy: impact of audio instruction and audio-visual biofeedback on respiratory-gated radiotherapy. Int J Radiat Oncol Biol Phys 2006;65:924–33. [PubMed: 16751075]

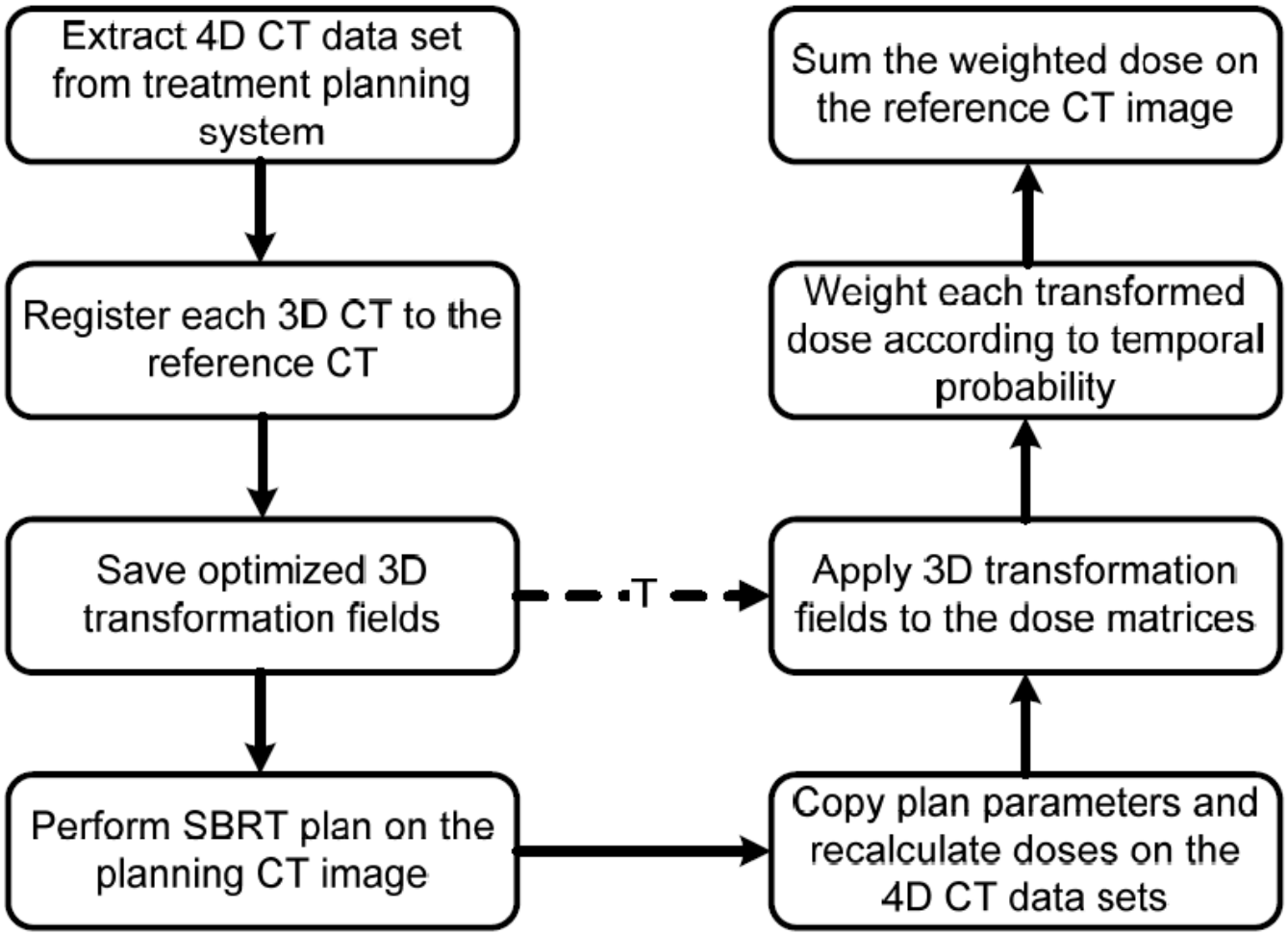

Figure 1.
Flow chart of the entire process of 4D dose calculation.

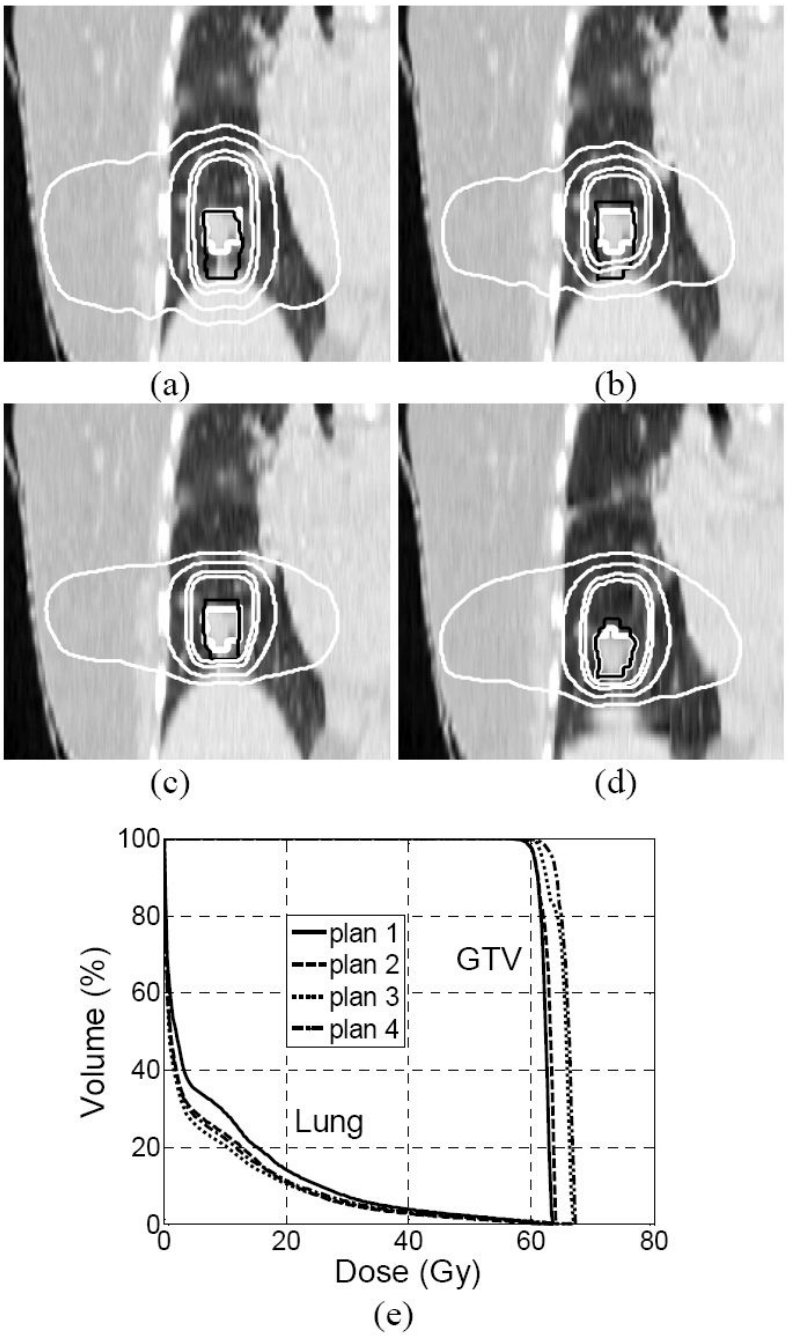

Figure 2.

Isodose lines (100%, 85%, 50% and 20%) corresponding to 4D doses (thin white lines) and target contours (thick white and thin black curves) for a representative patient resulting from (a) plan 1 with GTV at end exhale and GTV_{FB} shown, (b) plan 2 with GTV at end-exhale and ITV shown, (c) plan 3 with GTV at end-exhale and ITV_{ex} shown and (d) plan 3 with GTV at end-inhale and ITV_{in} shown. Note that plans 1-3 were calculated at end-exhale and plan 4 was calculated at end-inhale. (e) DVHs corresponding to plans 1-4.

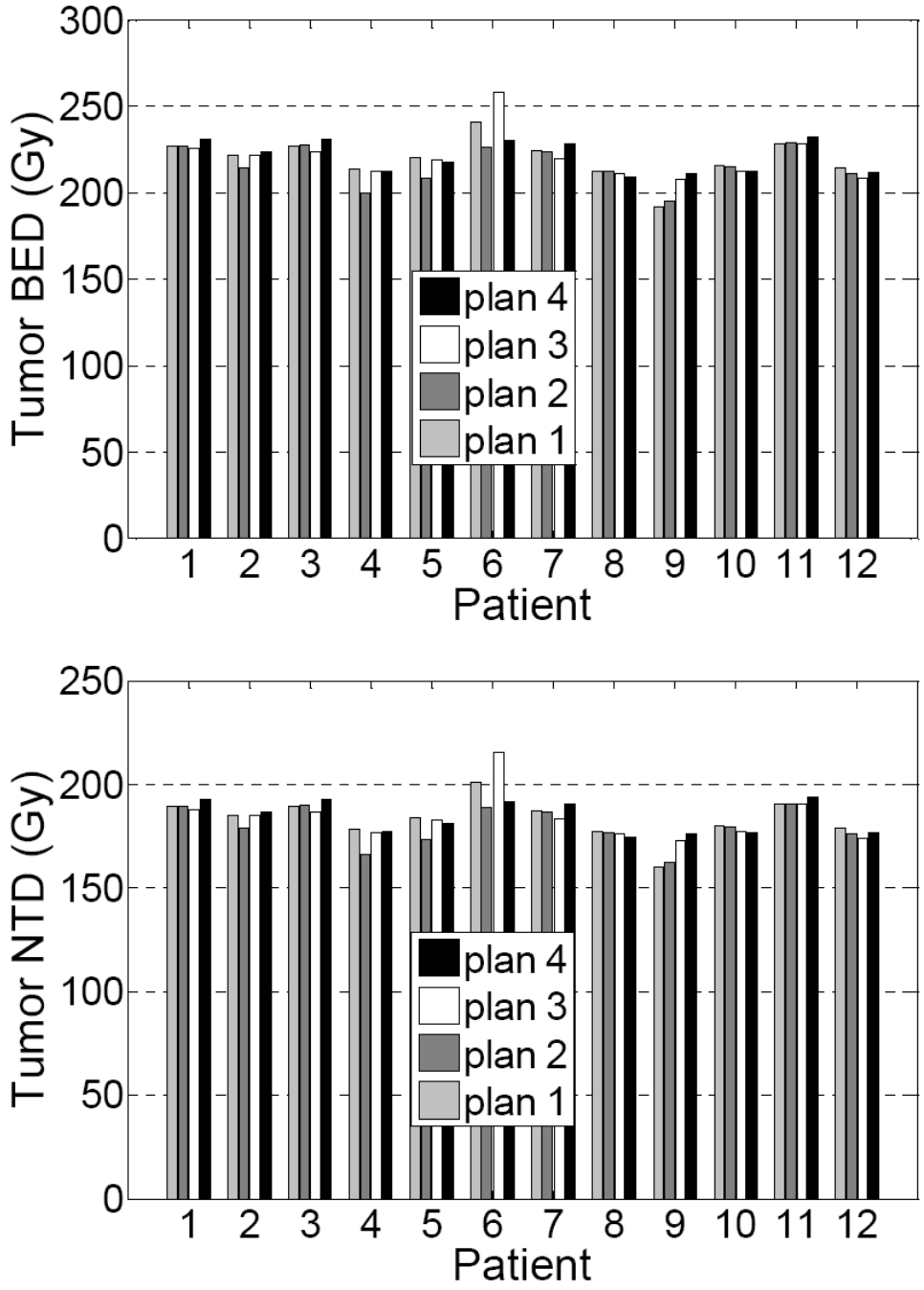

Figure 3.
Mean BED and mean NTD of the tumors resulting from the 4 SBRT plans for the 12 patients.

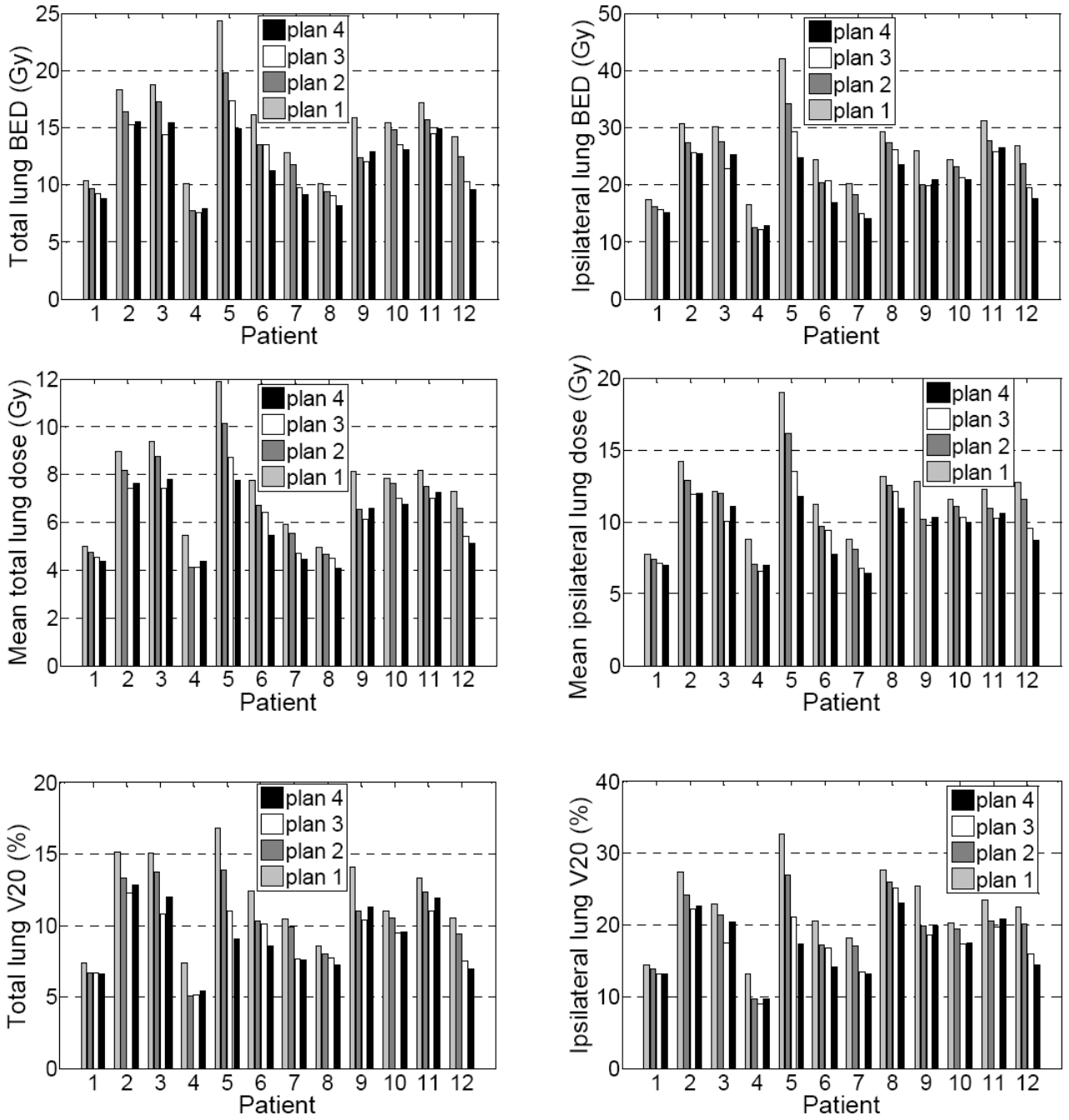

Figure 4.
Mean BED, mean lung dose, and V20 of the total lungs (left) and the ipsilateral lungs (right) of the 4 plans for the 12 patients.

Table 1

Summary of the 4 SBRT plans. For plan 1, GTV_{FB} was drawn on the free breathing (FB) CT image. ITV of plan 2 is a union GTVs delineated on 10 4D CT images. The ITV_{ex} of plan 3 and ITV_{in} of plan 4 are the unions of GTVs whose corresponding respiratory phases are within the phase-based gating window at end-exhale and end-inhale respectively. The structure volumes (GTV_{FB} or ITV and PTV) were averaged over the 12 patients.

Plan #	Plan CT	Definition of PTV	4D CT images	Number of plans	Averaged structure Volume (cc)	
					GTV_{FB} or ITV	PTV
1	FB	GTV_{FB} + 5-mm radial and 10-mm craniocaudal margin	10	11	47.3±35.2	123.5±71.0
2	FB	ITV + 0.5 cm uniform margin	10	11	52.7±38.6	112.4±67.0
3	EE	ITV_{ex} + 0.5 cm uniform margin	3 to 5	4 to 6	36.3±28.2	85.5±52.3
4	EI	ITV_{in} + 0.5 cm uniform margin	3 to 5	4 to 6	37.6±29.4	87.6±53.4

Table 2

Tumor volume (at end-exhale), location, and the amplitude of the motion of the center-of-mass (COM) of the GTVs as determined from 4D CT imaging.

Patient #	Volume (cm^3) (GTV_{ex})	Location	Motion (cm)
1	16.0	Right, low lobe	0.9
2	7.3	Right, low lobe	0.8
3	57.4	Left, low lobe	1.6
4	7.9	Right, middle lobe	0.9
5	56.6	Right, middle lobe	1.6
6	12.7	Right, middle lobe	0.8
7	37.1	Right, low lobe	1.1
8	42.7	Left, low lobe	1.0
9	6.3	Right, low lobe	1.1
10	19.6	Right, low lobe	1.1
11	81.3	Left, low lobe	1.0
12	22.5	Left, low lobe	1.7

Table 3

Absolute changes in mean BED, mean NTD and mean delivered dose for the tumors, mean BED, mean NTD, mean delivered dose, and V20 for the total lung and ipsilateral lung in plans 2-4 compared with plan 1 averaged over the 12 patients.

		Plan 1 as reference		
		Plan 2	**Plan 3**	**Plan 4**
Tumor	BED (Gy)	-4.0±6.2 (p=0.05)	0.9±7.6 (p=0.69)	1.0±7.2 (p=0.63)
	NTD (Gy)	-3.3±5.1 (p=0.05)	0.7±6.3 (p=0.69)	0.9±6.0 (p=0.63)
	Mean dose (Gy)	-0.7±1.1 (p=0.05)	0.2±1.4 (p=0.70)	0.2±1.3 (p=0.62)
Lung	BED (Gy)	-1.9±1.2 (p<0.01)	-3.1±1.6 (p<0.01)	-3.5±2.1 (p<0.01)
	NTD (Gy)	-1.6±1.0 (p<0.01)	-2.6±1.3 (p<0.01)	-2.9±1.8 (p<0.01)
	Mean dose (Gy)	-0.8±0.5 (p<0.01)	-1.5±0.8 (p<0.01)	-1.6±1.0 (p<0.01)
	V20 (%)	-1.5±1.0 (p<0.01)	-2.7±1.4 (p=0.01)	-2.8±1.8 (p<0.01)
Ipsilateral Lung	BED (Gy)	-3.4±2.0 (p<0.01)	-5.4±2.9 (p<0.01)	-6.2±3.9 (p<0.01)
	NTD (Gy)	-2.8±1.6 (p<0.01)	-4.5±2.4 (p<0.01)	-5.2±3.3 (p<0.01)
	Mean dose (Gy)	-0.9±1.3 (p=0.04)	-2.1±1.3 (p<0.01)	-2.5±1.9 (p<0.01)
	V20 (%)	-2.7±1.7 (p<0.01)	-4.9±2.6 (p<0.01)	-5.2±3.7 (p<0.01)

Table 4

Absolute difference in mean BED, mean NTD and mean delivered dose for the tumors, mean BED, mean NTD, mean delivered dose, and V20 for the total lung and ispilateral lung in plans 3-4 with respect to plan 2, and plan 4 with respect to plan 3, averaged over the 12 patients.

		Plan 2 as reference		**Plan 3 as reference**
		Plan 3	**Plan 4**	**Plan 4**
Tumor	BED (Gy)	4.9±10.6 (p=0.14)	5.0±5.8 (p=0.01)	0.1±9.6 (p=0.96)
	NTD (Gy)	4.1±8.9 (p=0.14)	4.2±4.8 (p=0.01)	0.1±8.0 (p=0.96)
	Mean dose (Gy)	0.9±1.9 (p=0.13)	0.9±1.1 (p=0.01)	0.0±1.7 (p=0.93)
Total lung	BED (Gy)	-1.2±1.0 (p<0.01)	-1.6±1.5 (p<0.01)	-0.4±1.1 (p=0.25)
	NTD (Gy)	-1.0±0.8 (p<0.01)	-1.3±1.2 (p<0.01)	-0.3±0.9 (p=0.25)
	Mean dose (Gy)	-0.6±0.5 (p<0.01)	-0.8±0.7 (p<0.01)	-0.1±0.5 (p=0.31)
	V20 (%)	-1.2±1.1 (p<0.01)	-1.3±1.5 (p=0.01)	-0.1±1.0 (p=0.82)
Ipsilateral lung	BED (Gy)	-2.1±1.8 (p<0.01)	-2.9±2.8 (p<0.01)	-0.8±2.1 (p=0.19)
	NTD (Gy)	-1.7±1.5 (p<0.01)	-2.4±2.3 (p<0.01)	-0.7±1.7 (p=0.19)
	Mean dose (Gy)	-1.3±0.9 (p<0.01)	-1.6±1.3 (p<0.01)	-0.3±0.9 (p=0.22)
	V20 (%)	-2.2±1.8 (p<0.01)	-2.5±2.9 (p=0.01)	-0.3±1.9 (p=0.54)